Published by Avanti Publishers

Journal of Advanced Thermal Science Research

ISSN (online): 2409-5826

# Flow and Heat Transfer Performance of Liquid Metal in Mini-Channel and Verification of Geometric Parameter Optimization

Liujin Xiang[1,2], Shuo Yang[1,2], Qi Wang[1,2], Jian Wu[1,2,*]

[1]School of Energy Science and Engineering, Harbin Institute of Technology, Harbin 150001, PR China

[2]Heilongjiang Key Laboratory of Micro-and Nano-scale Fluid Flow and Heat Transfer, Harbin 150001, PR China

## ARTICLE INFO

*Article Type*: Research Article

*Guest Editor*: *Xiaohui Yu*

*Keywords*:
Liquid metal
Mini-channel
Flow and heat transfer
Parameter optimization

*Timeline*:
Received: September 07, 2023
Accepted: November 01, 2023
Published: December 20, 2023

*Citation*: Xiang L, Yang S, Wang Q, Wu J. Flow and heat transfer performance of liquid metal in mini-channel and verification of geometric parameter optimization. J Adv Therm Sci Res. 2023; 10: 23-40.

*DOI*: https://doi.org/10.15377/2409-5826.2023.10.3

## ABSTRACT

With the rapid development of the electronics industry, the power of devices continues to rise, and seeking more efficient cooling technologies has become a key challenge in various applied scenarios. This study contributes to a novel and efficient heat dissipation method for chips employing liquid metal as a coolant. In this paper, the flow and heat transfer performance of a novel liquid metal ($Ga_{61}In_{25}Sn_{13}Zn_1$) in a mini-channel heat sink is conducted. Using pressure difference, pump power, and total thermal resistance as object parameters, a comprehensive optimization about $H_p$ (channel height), $W_c$ (channel width), $W_w$ (wall thickness), and $t_b$ (base thickness) is presented. The optimized parameter combination is $H_p$ = 7 mm, $W_c$ = 0.6 mm, $W_w$ = 0.4 mm, and $t_b$ = 0.2 mm. Furthermore, all of the optimization parameters are verified through the design method of orthogonal experiments.

*Corresponding Author
Email: jian.wu.85@hotmail.com
Tel: +(86) 0451 86402324

©2023 Xiang *et al*. Published by Avanti Publishers. This is an open access article licensed under the terms of the Creative Commons Attribution Non-Commercial License which permits unrestricted, non-commercial use, distribution and reproduction in any medium, provided the work is properly cited. (http://creativecommons.org/licenses/by-nc/4.0/)

# 1. Introduction

The integration and power consumption of electrical devices continue to increase as does the development of technology [1-3]. Examples include laser diodes [4-6], fuel cells [7, 8], high-power devices [9, 10], and so on. Efficient heat dissipation techniques capable of avoiding thermal barrier phenomena have garnered widespread attention [11-14]. Researchers have proposed a variety of active cooling methods and passive cooling methods to dissipate heat generated by electrical devices [15, 16]. While active cooling technology makes use of coolants and all kinds of enhanced heat transfer techniques, passive cooling technology is focused on improving the performance of the materials of the heat sink [17-20]. Among active cooling methods, air cooling is a traditional solution scheme suitable for scenarios with a heat flux below 10 W/m$^2$ [21, 22]. The two primary methods for dealing with heat dissipation issues at present are heat pipes and water cooling [23, 24]. However, both of them are commonly applied in cooling scenarios where the heat flux density is less than 100 W/cm$^2$, which is insufficient for the demands of rapidly increasing power [25, 26]. Commonly, electrical devices need to be kept at temperatures below 70 °C to ensure system stability and reliability [27-29], which further highlights the need for an effective cooling technique.

As a result, literature has reported various kinds of improved heat transfer methods [30-32]. Mini-channel cooling which was originally introduced by Tuckerman and Pease [33] in 1981 has drawn more attention due to its tiny structure and superior heat transfer capacity [34-37], the lower thermal conductivity of the coolant (usually water) restricts further improvements in heat transfer capacity. In recent years, liquid metals have attracted more focus in the fields of cooling owing to their excellent conductivity [37, 38]. Furthermore, its superior fluidity, conductivity, lower melting point, and higher boiling point are capable of performing well under situations of extreme heat flux [39, 40]. So that, liquid metal is widely adopted as a promising coolant in various heat dissipation research, such as commercial CPU heat dissipation [26, 41], high-power LED equipment thermal management [42, 43], high-power laser diode cooling [44], supersonic ramjet regenerative cooling [45, 46], chip cooling [47, 48], and phase change and energy storage materials [49-53].

Since Liu *et al.* [53]. utilized them for the first time to cool electronic equipment in 2002, numerous studies [54-57] have examined the usage of liquid metals in electrical device cooling. Liu *et al.* [58] introduced of a chip cooling method based on liquid metal in 2005, which employs an electromagnetic to pump coolant. Compared to conventional cooling techniques, liquid metals have a significant capacity for heat dissipation because of their superior fluidity and conductivity. In 2007, Ma *et al.* [59] designed a waste heat-powered liquid metal heat dissipation system. The chip temperature decreased dramatically using the self-powered approach from 91.5 °C to 62.5 °C at a heating power consumption of 25 W. In 2011, Li *et al.* [60] confirmed the feasibility of using the thermosiphon effect to drive liquid metal for electronic device heat dissipation, where the waste heat that needs to be released drives the coolant to operate. Based on the results, by implementing this method, a heat load of 42.1 W is capable of maintaining the heat source temperature at 87.7 °C. In 2019, Zhang *et al.* [61] employed a self-designed compact DC-EMP (electromagnetic pump) and chose Galinstan as the coolant to achieve thermal management of high heat flux (300 W/cm$^2$) and high-power (1500 W) equipment. To cool high-power laser diode arrays, Zhang *et al*. [62] used vascularized liquid metal, resulting in enhanced thermal management effects. Deng *et al.* [63] recently developed a dual-stage multi-channel liquid metal cooling system in 2022. The liquid metal cooling sub-system component serves as the first stage to achieve effective cooling of the chip, while the water-cooled part serves as the second stage to reduce costs. Additionally, the electromagnetic pump installed for each liquid metal cycle makes it simple to control chip temperature, resulting in a uniform temperature distribution of the chip. The aforementioned [53-63] research demonstrates that liquid metals have an excellent capacity for heat dissipation.

In addition, researchers are concentrating on the flow and heat transfer performance of liquid metals in mini-channel heat sinks. Yang *et al.* [38] conducted numerical simulation research on the flow and heat transfer capacity of liquid metal and water in micro/mini channels, and selected different correlation equations for theoretical analysis. The results show that liquid metals exhibit better flow and heat transfer capability in mini channels compared to water. In another study, Muhammad *et al.* [64] studied the effects of different factors such as *Re*, gallium alloys, and various base materials on the performance of minichannel heat sinks. According to the results, GaIn alloys have minimized flow resistance, and the conductivity of the substrate significantly affects the

thermal resistance of minichannel. In addition, Chen *et al.* [65] designed a top-slotted microchannel to address the drawback of higher liquid metal flow resistance in microchannel. According to the findings, the consumption of pump power lowers as slot height rises, with a minimum reduction of 16.5% when compared to the standard channel. And the total heat resistance has a trend of initially decreasing and then increasing. Yu *et al.* [66] provided heat transfer correlations for multiple flow directions based on their numerical research on laminar heat transfer of liquid metal under bottom heating conditions. The results showed that, under the same *Ra* number, the heat flux of both upward and lateral flow increased continually with aspect ratio, but the downward flow showed an opposite tendency.

Furthermore, a variety of studies on the parameter optimization of mini-channel heat sinks have been carried out by researchers. Orhan [54] performed a multi-objective optimization of the mini-channel heat sink to determine the most suitable combination of parameters, heat sink material, and coolant. Muhammad *et al.* [67] conducted a numerical simulation study on the laminar flow and heat transfer performance of liquid metal in mini-channels. The results show that the flow resistance depends on the channel height, channel width, and coolant velocity, and channels with lower aspect ratios have superior heat transfer capacity. The performance of microchannel heat exchangers in lithium-ion batteries was investigated by Liu *et al.* [68], who also developed an original tree-shaped heat sink structure. Based on mini-channel heat sinks, Deng *et al.* [69] developed a dual-sided heat dissipation system for high-power devices. Then they employed numerical simulation to optimize the structure of the microchannel and conducted experiments to verify the heat dissipation capacity. Results showed that the arrangement of staggered fins enhanced heat transfer performance. Applying ANN and NSGA-II approaches, Mathiyazhagan *et al*. [70] optimized the heat sink in a multi-objective way, obtaining a structure that minimized pressure loss and thermal resistance while maintaining vertical coolant delivery. Water-cooled microchannel electronic heat exchanger was the topic of topology optimization by Zou *et al.* [71] They further proposed a Pareto frontier-based heat exchanger design strategy, which was confirmed by a three-dimensional numerical simulation.

Our previous work [67] focused on typical heat sink models using Galinstan as the coolant and obtained its flow and heat transfer characteristics. This work employs a novel liquid metal ($Ga_{61}In_{25}Sn_{13}Zn_1$) as a coolant to research its performance on thermal management. In the present study, a numerical model based on ANSYS-Fluent for solving the flow and heat transfer process in microchannel heat sinks was established and validated. The influence of structural parameters of mini-channel on heat dissipation capacity was comprehensively discussed, and the optimal parameter combination for heat transfer capacity was obtained, which was verified through orthogonal experiments. The remainder of this paper is organized as follows: section 2. introduces the physical and numerical models, section 3. discusses the results in detail, the validation of optimization parameters is shown in section 4. , and the final section summarizes the conclusions.

# 2. Physical and Numerical Model

## 2.1. Physical Model

Regarding the research content of this paper, a typical chip size, which is set to $W \times L$ = 20 mm×20 mm, is considered and the top cover plate provides a closed channel for flow. Coolant flows along the positive $x$ direction. So, the inlet and outlet are on the plane with $x$ = 0 mm and $x$ = 20 mm, respectively. The bottom surface of the base is located in a plane with $z$ = 0 mm and the other external surfaces are treated as isolated walls. Fig. (**1**) shows the geometric design parameters of a single calculation unit, where $H$ and $W_c$ are channel height and channel width, respectively. The wall thickness of the channel separating the two mini-channels is defined as $W_w$, which acts like a fin, while $t_b$ is the thickness value of the base plate.

## 2.2. Governing Equations

Before conducting numerical calculations, the following assumptions are considered [67, 72-75]:

(1) In all cases considered in this paper, the *Re* number of fluid flow is less than 1700, so the flow of the fluid in the mini-channel is laminar.

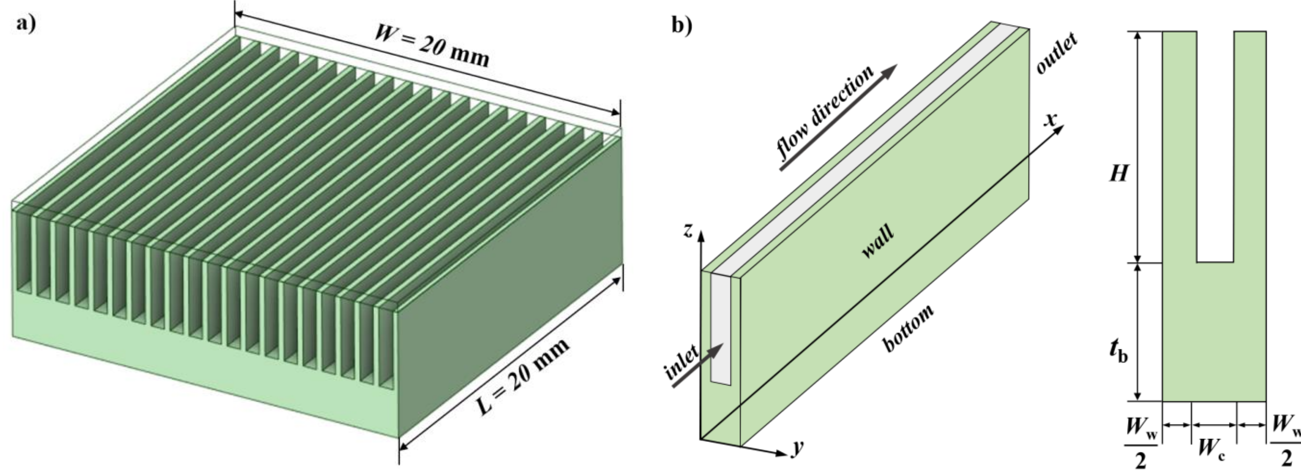


**Figure 1:** (**a**) 3D schematic diagram, and (**b**) Computational domain [67].

(2) Consider the flow in the mini-channel as a three-dimensional incompressible steady-state flow.

(3) Ignore the influence of volumetric forces.

(4) The thermophysical properties of the fluid are constant, and viscous dissipation is ignored.

(5) All mini-channels are identical, so only a single computational unit is considered in numerical simulation.

Following the previous assumptions, the governing equations of the fluid domain can be expressed as follows;

Continuity Equation:

$$\nabla \cdot \vec{U} = 0 \tag{1}$$

Momentum Equation:

$$\rho(\vec{U} \cdot \nabla\vec{U}) = -\nabla p + \nabla(\mu\nabla\vec{U}) \tag{2}$$

Energy Equation:

$$\rho C_p(\vec{U} \cdot \nabla T) = k_l \nabla^2 T \tag{3}$$

For the solid domain, the 3D heat conduction equation is to be solved.

$$k_s \nabla^2 T_s = 0 \tag{4}$$

## 2.3. Boundary Conditions and Solution Method

The boundary conditions are shown in the Table **1**.

**Table 1: Boundary condition settings.**

| Boundary | Expression |
|---|---|
| Inlet | $x = 0$, $u = U_{in}$, $v = w = 0$, $T = T_{in}$ |
| Outlet | $x = 20$ mm, $P_{out} = 0$ |
| Bottom wall | $z=0$, $q = const$ |
| Solid & fluid interface | $T_l = T_s$, $-k_l(\frac{\partial T_l}{\partial n}) = -k_s(\frac{\partial T_s}{\partial n})$ |
| other wall | $-k_s(\frac{\partial T_s}{\partial \boldsymbol{n}}) = 0$ |

The numerical calculation work is completed on Fluent and applies Fluent Meshing for mesh generation. A dual precision solver is employed, and the SIMPLE algorithm is selected to couple pressure and velocity. Momentum, mass, and energy equations are solved using a pressure-based steady-state solver. The gradient term is discretized using the least squares method, while the spatial discretization of momentum and energy terms is carried out using a second-order upwind scheme.

The liquid metal used in this paper is $Ga_{61}In_{25}Sn_{13}Zn_1$, which has the advantages of good safety, non-toxicity, high boiling point, and low volatility. At room temperature, it is difficult for it to react with air or water, nor can it react with copper below 100 °C [65]. Consequently, copper alloy (UNS C11000) will be used as a channel material in our work. The thermophysical properties of coolant and channel material are shown in Table **2**.

**Table 2: Thermophysical properties of coolant and channel materials.**

| Material | Density (kg/m$^3$) | Thermal Conductivity (W/(m·K)) | Specific Heat (J/(kg·K)) | Dynamic Viscosity ×10$^{-3}$(kg/(m·s)) | *Pr* |
|---|---|---|---|---|---|
| $Ga_{61}In_{25}Sn_{13}Zn_1$ | 6380 | 35.5 | 320 | 2.4 | 0.021 |
| Copper alloy | 8910 | 391.1 | 393.5 | — | — |

## 2.4. Flow and Thermal Model

To better analyze the flow and heat transfer performance of liquid metal in mini-channel, the model of flow resistance and thermal resistance is developed. Pressure drop is the essential performance of the heat sink system [76]. Thus, pressure drop ($\Delta P$) and pump power ($W_{\mathrm{pp}}$) are defined as:

$$\Delta P = f\frac{L}{D_{\mathrm{h}}}\frac{\rho U^2}{2} \tag{5}$$

$$W_{\mathrm{pp}} = n\Delta P U W_{\mathrm{c}} H \tag{6}$$

Where $n$ is the number of channels and $D_{\mathrm{h}}$ is the hydraulic diameter, which can be calculated using the following equation:

$$D_{\mathrm{h}} = \frac{2W_{\mathrm{c}}H}{W_{\mathrm{c}} + H} \tag{7}$$

From equation (5), to calculate $\Delta P$, $f$ (friction coefficient) should be firstly determined. According to ref. [38, 67]. The following correlations [77] are employed to calculate $f$:

$$\begin{aligned} f_{\mathrm{app}}Re &= 21.04(x^+)^{-0.434}\alpha^{-0.01} \quad 0.001 < x^+ < 0.02 \\ f_{\mathrm{app}}Re &= 45.2(x^+)^{-0.202}\alpha^{-0.094} \quad 0.02 < x^+ < 0.1 \end{aligned} \tag{8}$$

Where $\alpha$ is the aspect ratio of the channel, and $x^+$ is the dimensionless length of the hydrodynamic entrance region:

$$\alpha = \frac{W_{\mathrm{c}}}{H} \tag{9}$$

$$x^+ = \frac{L}{D_{\mathrm{h}}Re} \tag{10}$$

Reynolds number is defined as:

$$Re = \frac{D_{\mathrm{h}}U_{\mathrm{in}}\rho}{\mu} \tag{11}$$

Where $\rho$ is the density of liquid metal and $\mu$ is the dynamic viscosity of liquid metal.

In this paper, a simplified one-dimensional thermal resistance model developed by Liu *et al.* [78] is employed. to examine the heat transfer efficiency within the mini-channel. This model assumes that the heat flux is only occurring in one direction, disregarding any transverse heat conduction in the mini-channel. The total thermal resistance is defined by equation (12).

$$R_{\mathrm{tot}} = \frac{\Delta T_{\mathrm{max}}}{Q} = \frac{T_{\mathrm{max}} - T_{\mathrm{in}}}{Q} \tag{12}$$

$$\Phi = q \cdot A_{\mathrm{b}} \tag{13}$$

Where $\Delta T_{max}$, $T_{max}$, and $T_{in}$ represent the maximum temperature difference within the mini-channel, the maximum temperature at the base, and the inlet temperature of the coolant, respectively. $q$ is the given constant heat flux density, and $A_b$ is the base area.

Total thermal resistance can be further divided into the conduction thermal resistance caused by upward heat conduction at the base of the mini-channel, the convective heat transfer thermal resistance caused by convective cooling in the mini-channel, and the thermal capacity thermal resistance caused by the temperature rise of the coolant itself:

$$R_{\mathrm{tot}} = R_{\mathrm{cond}} + R_{\mathrm{conv}} + R_{\mathrm{cap}} \tag{14}$$

Conductive thermal resistance ($R_{cond}$), convective thermal resistance ($R_{conv}$), and heat capacity thermal resistance ($R_{cap}$) are defined as:

$$R_{\mathrm{cond}} = \frac{t_{\mathrm{b}}}{k_{\mathrm{s}} W L} \tag{15}$$

$$R_{\mathrm{conv}} = \frac{1}{h A_{\mathrm{sf}}} = \frac{1}{n h L (W_{\mathrm{c}} + 2\eta_{\mathrm{f}} H)} \tag{16}$$

$$R_{\mathrm{cap}} = \frac{1}{m^* C_{\mathrm{p}}} = \frac{1}{n \rho U_{\mathrm{i}} H W_{\mathrm{c}} C_{\mathrm{p}}} \tag{17}$$

Where $k_s$ represents the thermal conductivity of the solid wall, $A_{sf}$ represents the actual heat transfer surface area, and $m^*$ represents the mass flow rate of the mini-channel flowing through. The fin efficiency is represented in equation (16), which is defined as equation (18). For the fin efficiency of a uniform cross-section straight fin, the expression is:

$$\eta_{\mathrm{f}} = \frac{tanh(mH)}{mH} \tag{18}$$

In the above equation, $H$ is the height of the fins, i.e., channel height, and $m$ is the dimensionless fin height, which can be calculated using the following equation:

$$m = \sqrt{\frac{2h}{k_{\mathrm{s}} W_{\mathrm{w}}}} \tag{19}$$

From equation (16), it can be found that to obtain the convective heat transfer resistance of the mini-channel, it is necessary to first know the convective heat transfer coefficient within the channel, which is related to the corresponding thermal development state. Therefore, the dimensionless length of hydrodynamic entrance region is defined as:

$$x^* = \frac{L}{D_{\mathrm{h}} Re Pr} \tag{20}$$

In this paper, the flow and heat transfer of liquid metal in mini-channel is all in the stage of fully developed. Therefore, equation (21) and (22) [51] is employed for calculation:

$$Nu_{\mathrm{fd}} = 8.235(1 - 2.0421\alpha + 3.0853\alpha^2 - 2.4765\alpha^3 + 1.0578\alpha^4 - 0.1861\alpha^5) \tag{21}$$

$$h = \frac{Nu_{\mathrm{fd}} k_{\mathrm{l}}}{D_{\mathrm{h}}} \tag{22}$$

Where $k_l$ is the thermal conductivity of the liquid metal.

### 2.5. Grid Independence and Model Validation

To ensure the accuracy of numerical calculations and obtain grid-independent results, grid independence verification is conducted. Five sets of grids were selected for verification, with the number of grids being 51273, 250983, 436948, 870582, and 1367573, respectively. The cases of $H$=3 mm, $t_b$=2 mm, $W_c$=0.6 mm, $W_w$=0.4 mm, and $U_i$=0.15 m/s were considered. The results of the verification are shown in Fig. (**2**). It can be seen that the maximum temperature of the heat source between Case 4 and Case 5 is consistent, with a deviation of only 0.002%. Under the balance of computational efficiency and accuracy, grid 4 is selected for numerical calculation.

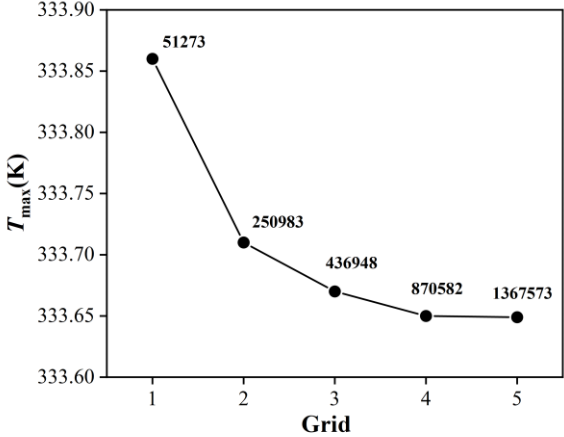


**Figure 2:** Grid independence verification.

In the following, a comparison was first made with the results obtained in the study [38], which simulated the laminar flow of gallium alloy (Galinstan)in a mini-channel. Select the physical parameters of the coolant in this study, maintain $W_c$=0.6 mm, $W_w$=0.4 mm, $t_b$=2 mm, $U_i$=0.15 m/s unchanged, and gradually increase $H$ from 3 mm to 9 mm. Fig. (**3**) shows the comparison between our numerical simulation results and the literature results. It can be seen that the maximum error does not exceed 2.63%, which reflects the reliability of the numerical calculation model established in this work.

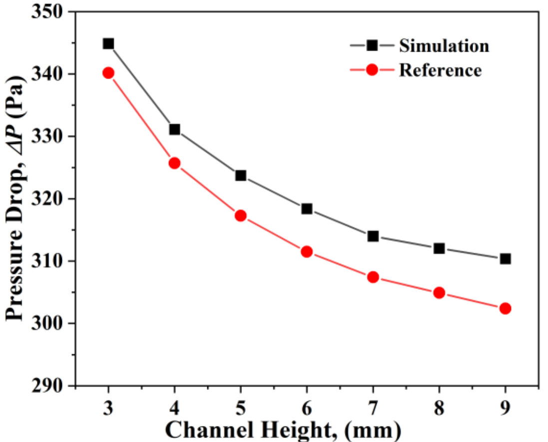


**Figure 3:** Model validation.

## 3. Results and Discussion

### 3.1. Effect of Channel Height

Fig. (**4**) shows the effect of $H$ (channel height) on both flow and heat transfer of the coolant. As shown in Fig. (**4a**), when $H$ increases from 2 mm to 10 mm, $\Delta T_{max}$ decreases from 57.40 K to 30.89 K, greatly enhancing the heat dissipation capacity of the mini-channel. Additionally, $\Delta P$ decreases by 18.16%, while $W_{pp}$ increases by 309%, as illustrated in Fig. (**4b**). On the one hand, according to equation (5), it can be observed that $\Delta P$ is inversely proportional to $D_h$, and when $H$ increases from 2 mm to 10 mm, $D_h$ increases from 0.92 mm to 1.13 mm. Consequently, $\Delta P$ decreases with the increase of $H$. On the other hand, $Q$ (volume flow rate) increases by 400% with the change of $H$. This implies that the increase in $Q$ is more significant than the decrease in $\Delta P$, resulting in an increase in $W_{pp}$ with the increase of $H$, as per equation (5).

Fig. (**4c**) illustrates the correlation between $R_{tot}$ and $q_{max}$ as $H$ varies. The variation trend of $R_{tot}$ is the same as $\Delta P$. In addition, as $H$ increases from 2 mm to 7 mm, $R_{tot}$ significantly decreases. However, as $H$ increases from 7 mm to 10 mm, $R_{tot}$ decreases more and more slowly. At the beginning, $q_{max}$ rapidly increases with the increase of $H$, and only gradually increases when $H$ reaches 7 mm. It implies that for $H > 7$ mm, the consumption of $W_{pp}$ will increase, but there will not be a significant improvement in heat transfer performance. The comparison of the theoretical and simulated thermal resistance is also shown in Fig. (**4c**). It illustrates how change trends in the simulation results are consistent with those found in the theoretical calculation. Error is primarily caused by the correlation of heat transfer. Nevertheless, employing the correlation here is adequate for qualitatively evaluating the trend of total thermal resistance. Based on the above discussion, $H_p$ = 7 mm is chosen as the optimized channel height value.

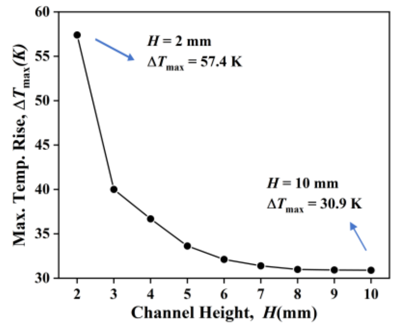


(**a**) Variation of maximum temperature rise at the base with channel height

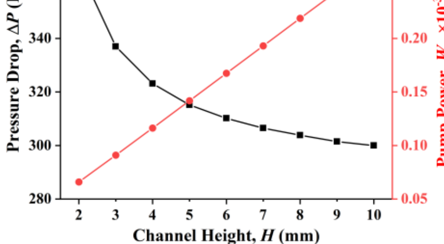


(**b**) Variation of pressure drop and pump power with channel height

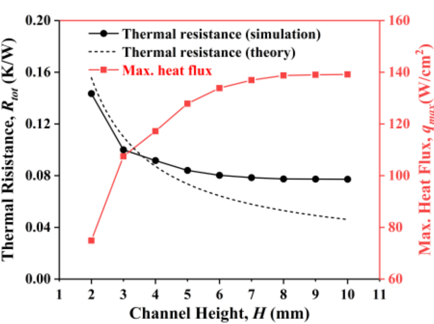


(**c**) Variation of total thermal resistance and maximum heat flux density with channel height

Calculate conditions: $W_c$ = 0.6 mm, $W_w$ = 0.4 mm, $t_b$ = 2 mm, and $U_i$ = 0.15 m/s

**Figure 4:** Effect of channel height on mini-channel performance.

### 3.2. Effect of Channel Width

Fig. (**5**) shows the effect of $W_c$ on the flow and heat transfer performance of the mini-channel. As $W_c$ increases from 0.3 mm to 0.6 mm, $\Delta T_{max}$ initially decreases and then increases, with little overall change, as shown in Fig. (**5a**). In addition, upon comparing Fig. (**4a**) and Fig. (**5a**), it can be inferred that the effect of $H$ on heat transfer performance is more pronounced than the effect of $W_c$.

Fig. (**5b**) illustrates the relationship between $W_{pp}$ and $\Delta P$ concerning $W_c$. The results indicate that both $W_{pp}$ and $W_c$ decrease as the increase of $W_c$, but the decreasing trend gradually slows down. When $W_c$ changes from 0.3 mm to 1.0 mm, $\Delta P$ decreases from 1057.3 Pa to 143 Pa. Comparing Fig. (**4b**) and Fig. (**5b**), it is evident that $W_c$ has a greater impact on $\Delta P$ compared to $H$. Fig. (**5c**) shows that $q_{max}$ initially increases and then decreases with increasing of $W_c$, reaching its maximum value (136.9 W/cm$^2$) at 0.6 mm. On the other hand, $R_{tot}$ exhibits the opposite trend, with the minimum value (0.0785 K/W) at 0.6 mm. Mini-channel has the best heat transfer performance when $W_c$ is 0.6 mm. In summary, $W_c$ = 0.6 mm is chosen as the optimized channel width value.

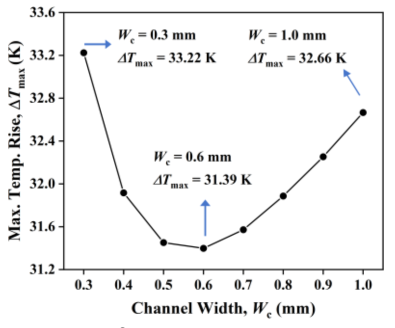


(**a**) Variation of maximum temperature rise at the base with channel width

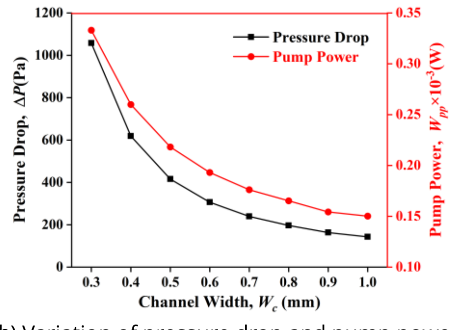


(**b**) Variation of pressure drop and pump power with channel width

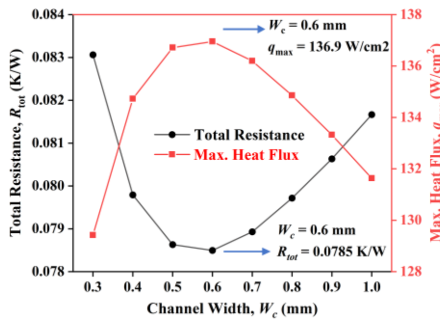


(**c**) Variation of total thermal resistance and maximum heat flux density with channel width

Calculate conditions: $H = 7$ mm, $W_w = 0.4$ mm, $t_b = 2$ mm, and $U_i = 0.15$ m/s

**Figure 5:** Effect of channel width on mini-channel performance.

### 3.3. Effect of Wall Thickness

Fig. (**6**) presents the impact curve of $W_w$ on the heat transfer performance. The result indicates that the effect of $W_w$ on the heat transfer performance of the mini-channel is similar to $W_c$, with a critical value. As depicted in Fig. (**6a**), this critical value is approximately around 0.4 mm. When $W_w$ is below this critical value, $\Delta T_{max}$ decreases from 36.19 K to 31.39 K as $W_w$ increases. Conversely, when $\Delta T_{max}$ exceeds this critical value, it increases again to 34.75 K.

Fig. (**6b**) shows the variation of $R_{tot}$ and $q_{max}$ with $W_w$. It can be seen that when $W_w$ is less than 0.4 mm, $R_{tot}$ decreases and $q_{max}$ increases, leading to an enhancement in heat transfer. When $W_w$ =0.4 mm, the total thermal resistance reached a peak value, which is $R_{tot}$ =0.0785 K/W, and $q_{max}$ reached the maximum value, 136.9 W/cm$^2$. As $W_w$ increases beyond 0.4 mm, the heat transfer efficiency significantly decreases, resulting in an increase in $R_{tot}$ and a decrease in $q_{max}$. This is because $R_{cond}$ is related to the channel material, while $R_{cap}$ is related to flow rate and specific heat, so changes in $W_w$ will not cause changes in $R_{cond}$ and $R_{cap}$. For $R_{conv}$, the fin efficiency continues to increase with the increase of $W_w$, resulting in a decrease in $R_{conv}$ (from equations (15) - (17)). However, as $W_w$ increases, $R_{cond}$ inside the fins cannot be ignored, and it continuously increases with the increase of $W_w$. Hence, the interaction between $R_{conv}$ in the fin and the $R_{conv}$ results in such a trend of the variation of $R_{tot}$. Based on the analysis presented above, it is evident that the minimum $R_{tot}$ and $q_{max}$ of the mini-channel are both obtained at $W_w$ =0.4 mm. Therefore, 0.4 mm is chosen as the optimized $W_w$ value.

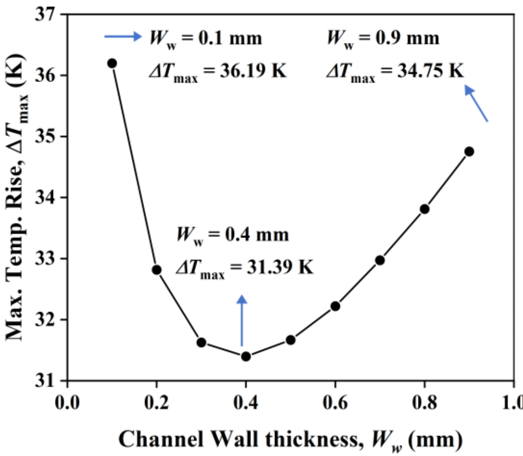


(**a**) Variation of maximum temperature rise at the base with wall thickness

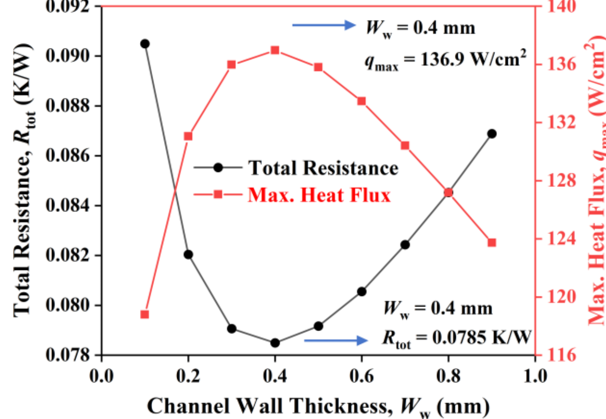


(**b**) Variation of total thermal resistance and maximum heat flux density with wall thickness

Calculate conditions: $H = 7$ mm, $Wc = 0.6$ mm, $t_b = 2$ mm, and $U_i = 0.15$ m/s

**Figure 6:** Effect of wall thickness on mini-channel performance.

### 3.4. Effect of Base Thickness

Based on the previous geometric parameter optimization results, the impact of $t_b$ (base thickness) on heat transfer performance is investigated and the results are shown in Fig. (**7**). By comparing Fig. (**7a**) and Fig. (**7b**), there is a critical value of approximately 0.2 mm, similar to the values for $W_c$ and $W_w$. When $t_b$ increases from 0.05 mm to 0.2 mm, $\Delta T_{max}$ shows a decrease of about 1 K. Additionally, $R_{tot}$ has also decreased from 0.0741 K/W to the minimum value of 0.0720 K/W, while $q_{max}$ increases from 145 W/cm$^2$ to the maximum value of 149.1 W/cm$^2$, indicating an enhancement in the heat transfer performance of the mini-channel. As $t_b$ further increases from 0.2 mm to 2 mm and $\Delta T_{max}$ rises again to 31.39 K, $R_{tot}$ increases again to 0.0785 K/W, and $q_{max}$ decreases to 136.9 W/cm$^2$.

According to equations (15) - (17), both $R_{conv}$ and $R_{cap}$ are independent of $t_b$. For the heat entering the base of the heat sink, it can be transferred to the coolant through two pathways. The first involves heat transfer from the bottom surface to the top surface, and the second involves heat transfer through the fins to the inner wall of the channel. In the first pathway, $R_{cond}$ increases with the increase of tb, resulting in a decrease in heat transfer. For the second pathway, heat transfer increases with the increase of $t_b$. When $t_b$ is less than 0.4mm, the second pathway dominates the heat transfer process, however, the first pathway dominates the heat transfer process, when $t_b$ is greater than 0.4mm. The balance of the two pathways leads to the trend of $R_{tot}$ variation. Therefore, 0.2 mm is chosen as the optimized value.

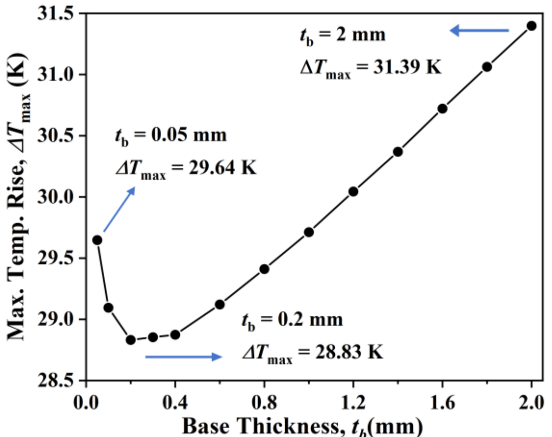


(**a**) Variation of maximum temperature rise at the base with base thickness

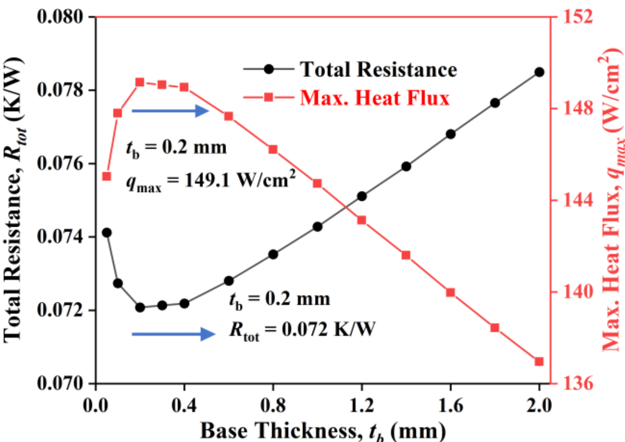


(**b**) Variation of total thermal resistance and maximum heat flux density with base thickness

Calculate conditions: $H$ = 7 mm, $Wc$ = 0.6 mm, $Ww$ =0.4 mm, and $U_i$ = 0.15 m/s

**Figure 7:** Effect of base thickness on mini-channel performance.

### 3.5. Effect of Inlet Velocity

Fig. (**8**) shows the variation of flow and heat transfer performance with $U_i$ in mini-channel after geometric optimization ($H$=7 mm, $W_w$=0.4 mm, $t_b$=0.2 mm, and $W_c$=0.6 mm). According to Fig. (**8a**) and Fig. (**8b**), it can be observed that as $U_i$ varies from 0.05 m/s to 0.40 m/s, $\Delta T_{max}$ decreases by 32.15 K, while $\Delta P$ increases from 94.27 Pa to 975.24 Pa. According to equation (6), it can be seen that $\Delta P$ increases with the increase of $U_i$. In addition, the results calculated using the theoretical correlation equation (8) and $W_{pp}$ are also shown in Fig. (**8b**), with a minimum relative error of only 1.6%, which further confirms the accuracy of the model.

The variations in $q_{max}$ and $R_{tot}$ with $U_i$ are shown in Fig. (**8c**). It becomes apparent that as $U_i$ increases, $R_{tot}$ decreases, while $q_{max}$ shows an opposite trend. It indicates that as $U_i$ increases, the erosion of the inner wall surface by coolant becomes more severe, resulting in an enhancement of $h$, thus $R_{conv}$ decreases from equations (15) - (17). $R_{cond}$ is independent of $U_i$, but an increase in $U_i$ means an increase in $m^*$, resulting in a decrease in $R_{cap}$

from 0.116 K/W to 0.0145 K/W. And the decrease gradually slows down, resulting in a smoother reduction in $R_{tot}$. Based on the analysis mentioned above, it can be concluded that under relatively high inlet speeds, it is possible to achieve a lower total thermal resistance by accepting a higher pressure drop, thus enhancing the heat transfer capability.

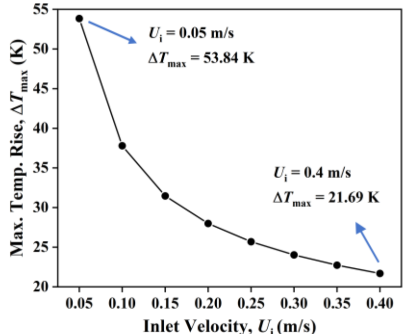


(**a**) Variation of maximum temperature rise at the base with inlet velocity

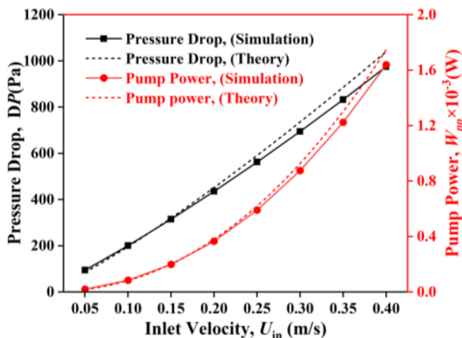


(**b**) Variation of pressure drop and pump power with inlet velocity

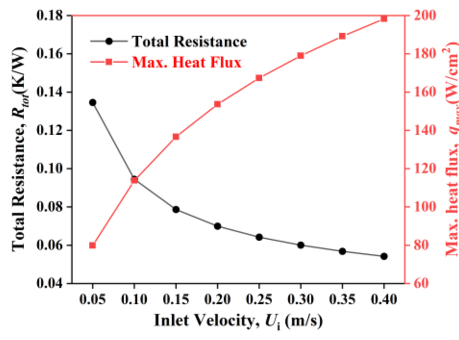


(**c**) Variation of total thermal resistance and maximum heat flux density with inlet velocity

Calculate conditions: $H$ = 7 mm, $W$c = 0.6 mm, $W$w =0.4 mm, and $t_b$ = 0.2 mm

**Figure 8:** Effect of inlet velocity on mini-channel performance.

# 4. Verification of Geometric Optimization Results

Based on the previous conversation regarding the impact of structure factors on the flow and heat transfer efficiency of the mini-channel, an approximate optimized structure parameter combination of the mini-channel is obtained: $H$=7 mm, $W_c$=0.6 mm, $W_w$=0.4 mm, and $t_b$=0.2 mm.

Based on the orthogonal experimental design approach, the accuracy of the numerical simulation results [79, 80] is performed. Use coefficients A, B, C, and D to represent channel height, channel width, channel wall thickness, and bottom plate thickness, respectively. Based on the previous results, four representative values were selected for A, B, C, and D as the four-level values. The factors and level tables obtained are shown in Table **3**.

**Table 3: Factors and levels.**

| Levels | Factors | | | |
|---|---|---|---|---|
| | A | B | C | D |
| | $H$ (mm) | $W_c$ (mm) | $W_w$ (mm) | $t_b$ (mm) |
| 1 | 4 | 0.5 | 0.3 | 0.2 |
| 2 | 5 | 0.6 | 0.4 | 0.3 |
| 3 | 6 | 0.7 | 0.5 | 0.4 |
| 4 | 7 | 0.8 | 0.6 | 0.5 |

Considering the number of factors of levels, the $L_{16}(4^5)$ orthogonal table was employed to conduct experimental arrangement, as shown in Table **4**. In the $L_{16}(4^5)$ notation, the number 5 represents five factors in the experiment. However, in this study, there are only four factors, so the last column in the Table is blank (Any two columns in the orthogonal table can be interchanged and blank columns are allowed to exist). The number 4 indicates that there are four levels or values for each factor, while 16 indicates the number of times the experiment needs to be conducted.

**Table 4: Arrange tests using $L_{16}$ ($4^5$) orthogonal table.**

| S.No. | Factors | | | | |
|---|---|---|---|---|---|
| | A | B | C | D | Blank |
| | $H$ (mm) | $W_c$ (mm) | $W_w$ (mm) | $t_b$ (mm) | |
| 1 | 1 | 2 | 3 | 2 | − |
| 2 | 3 | 2 | 1 | 4 | − |
| 3 | 2 | 3 | 3 | 4 | − |
| 4 | 4 | 3 | 1 | 2 | − |
| 5 | 1 | 4 | 1 | 3 | − |
| 6 | 3 | 4 | 3 | 1 | − |
| 7 | 2 | 1 | 1 | 1 | − |
| 8 | 4 | 1 | 3 | 3 | − |
| 9 | 1 | 3 | 4 | 1 | − |
| 10 | 3 | 3 | 2 | 3 | − |
| 11 | 2 | 2 | 4 | 3 | − |
| 12 | 4 | 2 | 2 | 1 | − |
| 13 | 1 | 1 | 2 | 4 | − |
| 14 | 3 | 1 | 4 | 2 | − |
| 15 | 2 | 4 | 2 | 2 | − |
| 16 | 4 | 4 | 4 | 4 | − |

Therefore, numerical calculations on a total of 16 combinations of four factors at four levels are conducted, and the results of $R_{tot}$ and $\Delta P$ are listed in Table **5**. It can be observed that combination 12 (4-2-2-1) with the smallest $R_{tot}$ (0.072131 K/W) has the best heat transfer performance, consistent with the previously optimized geometric structure. After comparison, it is found that in the 16 cases calculated in Table **5**, $\Delta P$ was within an acceptable range. Hence, the changes in heat transfer performance are focused on analysis.

To enhance the analysis of heat transfer performance, further calculations were conducted using the results in Table **5**. The of these calculations are presented in Table **5**. Where, $i$ ($i$=1, 2, 3, 4) represents the average impact of the $i$-th level, which is the average value of the $i$-th level of the factor in each column. Regarding the channel height, the maximum value occurs at $H$=4 mm and the minimum value is at $H$=7 mm, which is consistent with previous numerical simulation results. However, for variables $W_c$, $W_w$, and $t_b$, there are some discrepancies between Table **5** and those numerical simulations, which indirectly reflects the interaction among these factors. Furthermore, by calculating the range (i.e., the maximum difference between average influences), factor A has the largest range. Therefore, channel height has the greatest impact on the heat transfer performance of the mini-channel.

To verify the accuracy of the orthogonal design, additional numerical simulations are conducted. Select values of 7, 0.6, and 0.2 mm for factors A, B, and D while selecting levels 3 and 4 for factor C. Comparing the best combination of 4-2-2-1 and 4-2-3-1 results shows that $R_{tot}$ (0.072833 K/W) of combination 4-2-3-1 was greater than combination 4-2-2-1 (0.072131 K/W), which also verifies the accuracy of the orthogonal experimental design.

**Table 5: Analysis of the numerical simulation results.**

| S. No. | Factors | | | | Results | |
|---|---|---|---|---|---|---|
| | A | B | C | D | $R_{tot}$ (K/W) | $\Delta P$ (Pa) |
| | $H$ (mm) | $W_c$ (mm) | $W_w$ (mm) | $t_b$ (mm) | | |
| 1 | 1 | 2 | 3 | 2 | 0.091006 | 342.97 |
| 2 | 3 | 2 | 1 | 4 | 0.074337 | 330.69 |
| 3 | 2 | 3 | 3 | 4 | 0.079779 | 260.48 |
| 4 | 4 | 3 | 1 | 2 | 0.074100 | 251.46 |
| 5 | 1 | 4 | 1 | 3 | 0.082803 | 220.42 |
| 6 | 3 | 4 | 3 | 1 | 0.075193 | 208.67 |
| 7 | 2 | 1 | 1 | 1 | 0.077102 | 445.45 |
| 8 | 4 | 1 | 3 | 3 | 0.074062 | 435.53 |
| 9 | 1 | 3 | 4 | 1 | 0.092699 | 268.13 |
| 10 | 3 | 3 | 2 | 3 | 0.074376 | 256.71 |
| 11 | 2 | 2 | 4 | 3 | 0.084591 | 335.06 |
| 12 | 4 | 2 | 2 | 1 | 0.072131 | 327.16 |
| 13 | 1 | 1 | 2 | 4 | 0.090026 | 453.51 |
| 14 | 3 | 1 | 4 | 2 | 0.080813 | 440.03 |
| 15 | 2 | 4 | 2 | 2 | 0.077703 | 213.67 |
| 16 | 4 | 4 | 4 | 4 | 0.073555 | 205.47 |
| $\overline{R_1}$ | 0.089133 | 0.080501 | 0.077085 | 0.079281 | - | - |
| $\overline{R_2}$ | 0.079794 | 0.080516 | 0.078559 | 0.080905 | - | - |
| $\overline{R_3}$ | 0.076180 | 0.080238 | 0.080010 | 0.078958 | - | - |
| $\overline{R_4}$ | 0.073462 | 0.077313 | 0.082914 | 0.079424 | - | - |
| Range | 0.015671 | 0.003202 | 0.005828 | 0.001947 | - | - |

# 5. Conclusion

This study optimized and verified the geometric parameters of the mini-channel while numerically simulating the flow and heat transfer performance of the coolant. The following main conclusions were made:

1) The optimization parameter obtained through numerical simulation includes $H$=7 mm, $W_c$=0.6 mm, $W_w$=0.4 mm, and $t_b$=0.2 mm, and it is verified through orthogonal experimental design
2) With the optimal parameters mentioned in this paper, $Ga_{61}In_{25}Sn_{13}Zn_1$ can achieve a thermal management of 149.1W/cm$^2$, with a minimum thermal resistance of 0.072 K/W;
3) The geometric parameters of the mini-channel and the inlet velocity of the coolant both contribute to $R_{tot}$ and $\Delta P$. Among these parameters, $H$ has the most significant impact on overall performance while $W_c$ has a greater influence on $\Delta P$ compared to H;
4) Regarding heat transfer efficiency, there exists a critical value for $W_c$, $W_w$, and $t_b$. Near the critical value, the heat transfer temperature difference is minimized, resulting in the best heat transfer performance.

# Nomenclature

| | |
|---|---|
| $H$ | Channel height (m) |
| $L$ | Channel length (m) |
| $W$ | Heat sink width (m) |
| $W_w$ | Channel wall thickness (m) |
| $W_c$ | Channel width (m) |
| $t_b$ | Base thickness (m) |
| $C_p$ | Specific heat (J/(kg K)) |
| $U_i$ | Inlet velocity (m/s) |
| $Nu$ | Nusselt number |
| $Re$ | Reynolds number |
| $Pr$ | Prandtl number |
| $k$ | thermal conductivity (W/(m·K)) |
| $q_{max}$ | maximum heat flux density(W/m$^2$) |
| $h$ | heat transfer coefficient (W/(m·K)) |
| $\Delta T_{max}$ | maximum temperature rise at base (K) |
| $T$ | temperature (K) |
| $\Delta P$ | Pressure difference (Pa) |
| $W_{pp}$ | Pump power (W) |
| $R$ | Thermal resistance (K/W) |
| $f$ | Friction factor |
| $m^*$ | Mass flow rate (kg/s) |
| $D_h$ | Hydraulic diameter (m) |
| $A_b$ | Base area (m$^2$) |
| $A_{sf}$ | Heat transfer area (m$^2$) |
| $T_s$ | solid temperature (K) |
| $m$ | dimensionless height of the fin |
| $Q$ | volume rate (m$^3$/s) |
| $x^*$ | dimensionless length for thermal entrance region |
| $x^+$ | dimensionless length for hydrodynamic entrance region |

**Greek Letters**

| | |
|---|---|
| $\alpha$ | channel aspect ratio |
| $\rho$ | density (kg/m$^3$) |
| $\eta_f$ | fin efficiency |
| $\mu$ | dynamic viscosity (Pa·s) |
| $\Phi$ | thermal power (W) |

**Subscripts**

| | |
|---|---|
| cond | conduction |
| conv | convection |
| cap | capacity |
| tot | total |
| l | liquid metal |
| s | solid |

# Conflict of Interest

The authors declare that they have no known competing financial interests or personal relationships that could have appeared to influence the work reported in this paper.

# Funding

This work is supported by Fundamental Research Funds for the Central Universities, China (Grant No. AUGA9803500921).

# References

[1] Huynh PH, Zin Htoo K, Kariya K, Miyara A. Experimental investigation thermal performance of loop heat Pipe operating with different working fluids. J Adv Therm Sci Res. 2019; 6: 19-30. https://doi.org/10.15377/2409-5826.2019.06.3

[2] Li R, Wang Z, Wu Z, Ni J, He L, Xiong M, *et al.* Enhanced cooling performance of stacked chips by structural modification for fractal micro-protrusions. Appl Therm Eng. 2023; 236: 121416. https://doi.org/10.1016/j.applthermaleng.2023.121416

[3] Liu GL, Liu J. Convective cooling of compact electronic devices via liquid metals with low melting points. J Heat Transfer. 2021; 143: 050404. https://doi.org/10.1115/1.4050404

[4] Datta M, Choi H-W. Microheat exchanger for cooling high power laser diodes. Appl Therm Eng. 2015; 90: 266-73. https://doi.org/10.1016/j.applthermaleng.2015.07.012

[5] Baraty Beni S, Bahrami A, Salimpour MR. Design of novel geometries for microchannel heat sinks used for cooling diode lasers. Int J Heat Mass Transf. 2017; 112: 689-98. https://doi.org/10.1016/j.ijheatmasstransfer.2017.03.043

[6] Xiang L, Cheng Y, Yu X, Fan Y, Yang X, Zhang X, *et al. High*-performance thermal management system for high-power LEDs based on double-nozzle spray cooling. Appl Therm Eng. 2023; 231: 121005. https://doi.org/10.1016/j.applthermaleng.2023.121005

[7] Wang R, Liang Z, Souri M, Esfahani MN, Jabbari M. Numerical analysis of lithium-ion battery thermal management system using phase change material assisted by liquid cooling method. Int J Heat Mass Transf. 2022; 183: 122095. https://doi.org/10.1016/j.ijheatmasstransfer.2021.122095

[8] Qian Z, Li Y, Rao Z. Thermal performance of lithium-ion battery thermal management system by using mini-channel cooling. Energy Convers Manag. 2016; 126: 622-31. https://doi.org/10.1016/j.enconman.2016.08.063

[9] Kim K-S, Won M-H, Kim J-W, Back B-J. Heat pipe cooling technology for desktop PC CPU. Appl Therm Eng. 2003; 23: 1137-44. https://doi.org/10.1016/S1359-4311(03)00044-9

[10] Deng Y, Liu J. Hybrid liquid metal–water cooling system for heat dissipation of high power density microdevices. Heat and Mass Transfer. 2010; 46: 1327-34. https://doi.org/10.1007/s00231-010-0658-7

[11] Bahiraei M, Heshmatian S. Electronics cooling with nanofluids: A critical review. Energy Convers Manag. 2018; 172: 438-56. https://doi.org/10.1016/j.enconman.2018.07.047

[12] Li J, Lv L, Zhou G, Li X. Mechanism of a microscale flat plate heat pipe with extremely high nominal thermal conductivity for cooling high-end smartphone chips. Energy Convers Manag. 2019; 201: 112202. https://doi.org/10.1016/j.enconman.2019.112202

[13] Gupta R, Asgari S, Moazamigoodarzi H, Down DG, Puri IK. Energy, exergy and computing efficiency based data center workload and cooling management. Appl Energy. 2021; 299: 117050. https://doi.org/10.1016/j.apenergy.2021.117050

[14] Yuan X, Zhou X, Pan Y, Kosonen R, Cai H, Gao Y, *et al.* Phase change cooling in data centers: A review. Energy Build. 2021; 236: 110764. https://doi.org/10.1016/j.enbuild.2021.110764

[15] Li S, Zhang H, Cheng J, Li X, Cai W, Li Z, *et al.* A state-of-the-art overview on the developing trend of heat transfer enhancement by single-phase flow at micro scale. Int J Heat Mass Transf. 2019; 143: 118476. https://doi.org/10.1016/j.ijheatmasstransfer.2019.118476

[16] Bouchard A, Hodges T, Stephan M, Wu L, Koukoulas T, Green RG, *et al. Ther*mal gradients integrated on-chip by passive radiative cooling of silicon nitride nanomechanical resonators. Appl Therm Eng. 2023; 229: 120561. https://doi.org/10.1016/j.applthermaleng.2023.120561

[17] Peng J, Fang C, Shu Z, Gao D. Heat transfer modeling and development of on-chip active cooling and heating microfluidic. Cryobiology. 2017; 80: 190. https://doi.org/10.1016/j.cryobiol.2017.10.143

[18] Peng Y-H, Wang D-H, Li X-Y, Zhang Y. Cooling chip on PCB by embedded active microchannel heat sink. Int J Heat Mass Transf. 2022; 196: 123251. https://doi.org/10.1016/j.ijheatmasstransfer.2022.123251

[19] Hua W, Zhang L, Zhang X. Research on passive cooling of electronic chips based on PCM: A review. J Mol Liq. 2021; 340: 117183. https://doi.org/10.1016/j.molliq.2021.117183

[20] Liu Y, Zhang Z, Zhang N, Yuan Y, Phelan PE. Thermal buffering performance of passive phase change material micro-pillar array systems on temperature regulation of microfluidic chips. J Energy Storage. 2023; 58: 106424. https://doi.org/10. 1064241016/j.est.2022.

[21] Whelan BP, Kempers R, Robinson AJ. A liquid-based system for CPU cooling implementing a jet array impingement waterblock and a tube array remote heat exchanger. Appl Therm Eng. 2012; 39: 86-94. https://doi.org/10.1016/j.applthermaleng.2012.01.013

[22] Chernysheva MA, Yushakova SI, Maydanik YuF. Copper–water loop heat pipes for energy-efficient cooling systems of supercomputers. Energy. 2014; 69: 534-42. https://doi.org/10.1016/j.energy.2014.03.048

[23] Faghri A. Heat pipes: review, opportunities and challenges. Frontiers in Heat Pipes. 2014; 5: 1-48. https://doi.org/10.5098/fhp.5.1

[24] Agostini B, Fabbri M, Park JE, Wojtan L, Thome JR, Michel B. State of the art of high heat flux cooling technologies. Heat Transf Eng. 2007; 28: 258-81. https://doi.org/10.1080/01457630601117799

[25] Tawk M, Avenas Y, Kedous-Lebouc A, Petit M. Numerical and experimental investigations of the thermal management of power electronics with liquid metal mini-channel coolers. IEEE Trans Ind Appl. 2013; 49: 1421-9. https://doi.org/10.1109/TIA.2013.2252132

[26] Deng Y, Liu J. Design of practical liquid metal cooling device for heat dissipation of high performance CPUs. J Electron Packag. 2010; 132: 031009. https://doi.org/10.1115/1.4002012

[27] Liu D, Zhao F-Y, Yang H-X, Tang G-F. Thermoelectric mini cooler coupled with micro thermosiphon for CPU cooling system. Energy. 2015; 83: 29-36. https://doi.org/10.1016/j.energy.2015.01.098

[28] Zhang X-D, Yang X-H, Zhou Y-X, Rao W, Gao J-Y, Ding Y-J, *et al. Expe*rimental investigation of galinstan based minichannel cooling for high heat flux and large heat power thermal management. Energy Convers Manag. 2019; 185: 248-58. https://doi.org/10.1016/j.enconman.2019.02.010

[29] Sung MK, Mudawar I. Single-phase and two-phase hybrid cooling schemes for high-heat-flux thermal management of defense electronics. 2008 11th Intersociety Conference on Thermal and Thermomechanical Phenomena in Electronic Systems, IEEE; 2008, p. 121-31. https://doi.org/10.1109/ITHERM.2008.4544262

[30] Pati AR, Panda A, Lily, Munshi B, Kumar A, Sahoo A, *et al.* Dropwise evaporative cooling of hot water: A novel methodology to enhance heat transfer rate at very high surface temperatures. Int J Therm Sci. 2018; 127: 335-50. https://doi.org/10.1016/j.ijthermalsci.2018.01.028

[31] Nguyen CT, Roy G, Gauthier C, Galanis N. Heat transfer enhancement using $Al_2O_3$–water nanofluid for an electronic liquid cooling system. Appl Therm Eng. 2007; 27: 1501-6. https://doi.org/10.1016/j.applthermaleng.2006.09.028

[32] Youssef R, Kalogiannis T, Behi H, Pirooz A, Van Mierlo J, Berecibar M. A comprehensive review of novel cooling techniques and heat transfer coolant mediums investigated for battery thermal management systems in electric vehicles. Energy Rep. 2023; 10: 1041-68. https://doi.org/10.1016/j.egyr.2023.07.041

[33] Tuckerman DB, Pease RFW. High-performance heat sinking for VLSI. IEEE Electron Device Lett. 1981; 2: 126-9. https://doi.org/10.1109/EDL.1981.25367

[34] Lee D-Y, Vafai K. Comparative analysis of jet impingement and microchannel cooling for high heat flux applications. Int J Heat Mass Transf. 1999; 42: 1555-68. https://doi.org/10.1016/S0017-9310(98)00265-8

[35] Xie XL, Tao WQ, He YL. Numerical study of turbulent heat transfer and pressure drop characteristics in a water-cooled minichannel heat sink. J Electron Packag. 2007; 129: 247-55. https://doi.org/10.1115/1.2753887

[36] Qu W, Mudawar I. Experimental and numerical study of pressure drop and heat transfer in a single-phase micro-channel heat sink. Int J Heat Mass Transf. 2002; 45: 2549-65. https://doi.org/10.1016/S0017-9310(01)00337-4

[37] Wang H, Chen Z, Gao J. Influence of geometric parameters on flow and heat transfer performance of micro-channel heat sinks. Appl Therm Eng. 2016; 107: 870-9. https://doi.org/10.1016/j.applthermaleng.2016.07.039

[38] Yang X-H, Tan S-C, Ding Y-J, Liu J. Flow and thermal modeling and optimization of micro/mini-channel heat sink. Appl Therm Eng. 2017; 117: 289-96. https://doi.org/10.1016/j.applthermaleng.2016.12.089

[39] Miner A, Ghoshal U. Cooling of high-power-density microdevices using liquid metal coolants. Appl Phys Lett. 2004; 85: 506-8. https://doi.org/10.1063/1.1772862

[40] Bo G, Ren L, Xu X, Du Y, Dou S. Recent progress on liquid metals and their applications. Adv Phys X. 2018; 3: 1446359. https://doi.org/10.1080/23746149.2018.1446359

[41] Liu J, Deng Y-G, Deng Z-S. Recent advancement on liquid metal cooling for thermal management of computer chip. Vol. 4: Electronics and Photonics, ASMEDC; 2010, p. 161-6. https://doi.org/10.1115/IMECE2010-37640

[42] Deng Y, Liu J. A liquid metal cooling system for the thermal management of high-power LEDs. Int Commun Heat Mass Transf. 2010; 37: 788-91. https://doi.org/10.1016/j.icheatmasstransfer.2010.04.011

[43] Kim H, Chang S, Song Y. Flexible liquid metal display using 3-Aminopropyl triethoxysilane-treated light emitting diodes (LEDs) array. Microelectron Eng. 2022; 253: 111677. https://doi.org/10.1016/j.mee.2021.111677

[44] Vetrovec J. Quasi-passive heat sink for high-power laser diodes. In: Zediker MS, Ed. High-Power Diode Laser Technology and Applications VII, SPIE; 2009. https://doi.org/10.1117/12.808658

[45] Xu J, Cheng K, Dang C, Wang Y, Liu Z, Qin J, *et al. Perf*ormance comparison of liquid metal cooling system and regenerative cooling system in supersonic combustion ramjet engines. Energy. 2023; 275: 127488. https://doi.org/10.1016/j.energy.2023.127488

[46] Cheng K, Xu J, Dang C, Qin J, Jing W. Performance evaluation of fuel indirect cooling based thermal management system using liquid metal for hydrocarbon-fueled scramjet. Energy. 2022; 260: 125068. https://doi.org/10.1016/j.energy.2022.125068

[47] Liu J, Deng Y-G, Deng Z-S. Recent advancement on liquid metal cooling for thermal management of computer chip. Vol. 4: Electronics and Photonics, ASMEDC; 2010, p. 161-6. https://doi.org/10.1115/IMECE2010-37640

[48] Ma KQ, Liu J, Xiang SH, Xie KW, Zhou YX. Study of thawing behavior of liquid metal used as computer chip coolant. Int J Therm Sci. 2009; 48: 964-74. https://doi.org/10.1016/j.ijthermalsci.2008.08.005

[49] Nguyen Q-K, Ma J, Zhang P. Liquid metal-filled phase change composites with tunable stiffness: Computational modeling and experiment. Mech Mater. 2023; 183: 104702. https://doi.org/10.1016/j.mechmat.2023.104702

[50] Yang X-H, Tan S-C, Liu J. Numerical investigation of the phase change process of low melting point metal. Int J Heat Mass Transf. 2016; 100: 899-907. https://doi.org/10.1016/j.ijheatmasstransfer.2016.04.109

[51] Yang X-H, Tan S-C, Ding Y-J, Wang L, Liu J, Zhou Y-X. Experimental and numerical investigation of low melting point metal-based PCM heat sink with internal fins. Int Commun Heat Mass Transf. 2017; 87: 118-24. https://doi.org/10.1016/j.icheatmasstransfer.2017.07.001

[52] Yang X-H, Tan S-C, He Z-Z, Zhou Y-X, Liu J. Evaluation and optimization of low melting point metal PCM heat sink against ultra-high thermal shock. Appl Therm Eng. 2017; 119: 34-41. https://doi.org/10.1016/j.applthermaleng.2017.03.050

[53] Liu J, Zhou YX. A computer chip cooling method that uses low melting point metal and its alloys as the cooling fluid. 2002; China Patent 2131419.

[54] Kalkan O. Multi-objective optimization of a liquid metal cooled heat sink for electronic cooling applications. Int J Therm Sci. 2023; 190: 108325. https://doi.org/10.1016/j.ijthermalsci.2023.108325

[55] Sarowar MT. Numerical analysis of a liquid metal cooled mini channel heat sink with five different ceramic substrates. Ceram Int. 2021; 47: 214-25. https://doi.org/10.1016/j.ceramint.2020.08.124

[56] Guo W, Prasser H-M. Direct numerical simulation of turbulent heat transfer in liquid metals in buoyancy-affected vertical channel. Int J Heat Mass Transf. 2022; 194: 123013. https://doi.org/10.1016/j.ijheatmasstransfer.2022.123013

[57] Zhang X-D, Yang X-H, Zhou Y-X, Rao W, Gao J-Y, Ding Y-J, *et al.* Experimental investigation of galinstan-based minichannel cooling for high heat flux and large heat power thermal management. Energy Convers Manag. 2019; 185: 248-58. https://doi.org/10.1016/j.enconman.2019.02.010

[58] Liu J, Zhou Y-X, Lv Y-G, Li T. Liquid metal based miniaturized chip-cooling device driven by electromagnetic pump. Electronic and Photonic Packaging, Electrical Systems Design and Photonics, and Nanotechnology, ASMEDC; 2005, p. 501-10. https://doi.org/10.1115/IMECE2005-80188

[59] Ma K-Q, Liu J. Heat-driven liquid metal cooling device for the thermal management of a computer chip. J Phys D Appl Phys. 2007; 40: 4722-9. https://doi.org/10.1088/0022-3727/40/15/055

[60] Li P, Liu J. Self-driven electronic cooling based on thermosyphon effect of room temperature liquid metal. J Electron Packag. 2011; 133: 041009. https://doi.org/10.1115/1.4005297

[61] Rui Z, Hodes M, Lower N, Wilcoxon R. Water-based microchannel and galinstan-based minichannel cooling beyond 1 kW/cm2 heat flux. IEEE Trans Compon Packaging Manuf Technol. 2015; 5: 762-70. https://doi.org/10.1109/TCPMT.2015.2426791

[62] Zhang X-D, Li X-P, Zhou Y-X, Yang J, Liu J. Vascularized liquid metal cooling for thermal management of kW high power laser diode array. Appl Therm Eng. 2019; 162: 114212. https://doi.org/10.1016/j.applthermaleng.2019.114212

[63] Deng Y, Zhang M, Jiang Y, Liu J. Two-stage multichannel liquid–metal cooling system for thermal management of high-heat-flux-density chip array. Energy Convers Manag. 2022; 259: 115591. https://doi.org/10.1016/j.enconman.2022.115591

[64] Muhammad A, Selvakumar D, Iranzo A, Sultan Q, Wu J. Comparison of pressure drop and heat transfer performance for liquid metal cooled mini-channel with different coolants and heat sink materials. J Therm Anal Calorim. 2020; 141: 289-300. https://doi.org/10.1007/s10973-020-09318-2

[65] Chen Z, Qian P, Huang Z, Luo C, Liu M. Study on flow and heat transfer of liquid metal in a new top-slotted microchannel heat sink. IOP Conf Ser Earth Environ Sci. 2021; 621: 012054. https://doi.org/10.1088/1755-1315/621/1/012054

[66] Yu P, Ma W, Ma R, Guo Q, Yang X, Yuan Y. A numerical study of heat transfer in bottom-heated and side/top-cooled liquid metal layers with different aspect ratios. Ann Nucl Energy. 2022; 177: 109328. https://doi.org/10.1016/j.anucene.2022.109328

[67] Muhammad A, Selvakumar D, Wu J. Numerical investigation of laminar flow and heat transfer in a liquid metal cooled mini-channel heat sink. Int J Heat Mass Transf. 2020; 150: 119265. https://doi.org/10.1016/j.ijheatmasstransfer.2019.119265

[68] Liu H, Shi H, Shen H, Xie G. The performance management of a Li-ion battery by using tree-like mini-channel heat sinks: Experimental and numerical optimization. Energy. 2019; 189: 116150. https://doi.org/10.1016/j.energy.2019.116150

[69] Deng Z, Zhang S, Ma K, Jia C, Sun Y, Chen X, *et al. Nume*rical and experimental study on cooling high power chips of data centers using double-side cooling module based on mini-channel heat sink. Appl Therm Eng. 2023; 227: 120282. https://doi.org/10.1016/j.applthermaleng.2023.120282

[70] Shanmugam M, Sirisha Maganti L. Multi-objective optimization of parallel microchannel heat sink with inlet/outlet U, I, Z type manifold configuration by RSM and NSGA-II. Int J Heat Mass Transf. 2023; 201: 123641. https://doi.org/10.1016/j.ijheatmasstransfer.2022.123641

[71] Zou A, Chuan R, Qian F, Zhang W, Wang Q, Zhao C. Topology optimization for a water-cooled heat sink in micro-electronics based on Pareto frontier. Appl Therm Eng. 2022; 207: 118128. https://doi.org/10.1016/j.applthermaleng.2022.118128

[72] He P, Lu H, Fan Y, Ruan H, Wang C, Zhu Y. Numerical investigation on a lithium-ion battery thermal management system utilizing a double-layered I-shaped channel liquid cooling plate exchanger. Int J Therm Sci. 2023; 187: 108200. https://doi.org/10.1016/j.ijthermalsci.2023.108200

[73] Yao F, Guan X, Yang M, Wen C. Study on liquid cooling heat dissipation of Li-ion battery pack based on bionic cobweb channel. J Energy Storage. 2023; 68: 107588. https://doi.org/10.1016/j.est.2023.107588

[74] Song S, Liao Q, Shen W, Ruan Y, Xu J. Numerical study on laminar convective heat transfer enhancement of microencapsulated phase change material slurry using liquid metal with low melting point as carrying fluid. Int J Heat Mass Transf. 2013; 62: 286-94. https://doi.org/10.1016/j.ijheatmasstransfer.2013.03.013

[75] Chen Z, Qian P, Huang Z, Zhang W, Liu M. Study on flow and heat transfer of liquid metal in the microchannel heat sink. Int J Therm Sci. 2022; 183: 107840. https://doi.org/10.1016/j.ijthermalsci.2022.107840

[76] Charles J, Wang X, Romero CE, Neti S. Experimental characterization of low-temperature inorganic. phase change materials by differential scanning calorimetry. J Adv Therm Sci Res. 2019; 6: 71-84. https://doi.org/10.15377/2409-5826.2019.06.8

[77] Harms TM, Kazmierczak MJ, Gerner FM. Developing convective heat transfer in deep rectangular microchannels. Int J Heat Fluid Flow. 1999; 20: 149-57. https://doi.org/10.1016/S0142-727X(98)10055-3

[78] Liu D, Garimella S V. Analysis and optimization of the thermal performance of microchannel heat sinks. Int J Numer Methods Heat Fluid Flow. 2005; 15: 7-26. https://doi.org/10.1115/IPACK2003-35260

[79] Xie XL, Liu ZJ, He YL, Tao WQ. Numerical study of laminar heat transfer and pressure drop characteristics in a water-cooled minichannel heat sink. Appl Therm Eng. 2009; 29: 64-74. https://doi.org/10.1016/j.applthermaleng.2008.02.002

[80] Montgomery DC. Design and analysis of experiments. New York: John Wiley & Son; 2004.